J Mater Sci (2015) 50:4463–4476
DOI 10.1007/s10853-015-8987-z

$BiFeO_3$ thin films via aqueous solution deposition: a study of phase formation and stabilization

Nikolina Pavlovic[1] · Jan D'Haen[2] · Hiwa Modarresi[3] · Alexander Riskin[1] · Christopher De Dobbelaere[1] · Margriet J. Van Bael[4] · Kristiaan Temst[3] · An Hardy[1] · Marlies K. Van Bael[1]

Received: 8 November 2014 / Accepted: 20 March 2015 / Published online: 11 April 2015

Abstract This paper reports a thorough microstructural investigation of bismuth ferrite (BFO) thin films subjected to various processing conditions and discusses their influence on the stability of the $BiFeO_3$ perovskite phase. The formation of secondary phases in BFO thin films is studied as a function of annealing temperature and time, film thickness, Bi excess, and Ti substitution. While films annealed at 600 °C consist of the desired $BiFeO_3$ phase, higher temperatures induce the decomposition leading to a significant amount of secondary phases, particularly the iron-rich $Bi_2Fe_4O_9$ phase. A longer annealing time at 700 °C further enhances the decomposition of $BiFeO_3$. Qualitative microstructural analysis of the films is performed by electron backscattered diffraction which provides phase analysis of individual grains. The morphology of the single-crystalline $Bi_2Fe_4O_9$ grains that are embedded in the $BiFeO_3$ matrix drastically changes as a function of the film thickness. Nucleation of these $Bi_2Fe_4O_9$ grains probably occurs at the film/substrate interface, after which grain growth continues toward the surface of the film through the depletion of the BFO phase. Addition of Bi excess or the substitution of Fe with Ti in the precursor solutions significantly reduces the formation of an iron-rich secondary phase. Influence of the secondary phases as well as Ti substitution on magnetic properties of BFO films was investigated.

Introduction

Bismuth ferrite (BFO), as a material with unique ferroelectric and magnetic properties at room temperature, is a candidate for a wide range of applications in electronic devices, especially in the form of thin films [1]. $BiFeO_3$ is the only known multiferroic material with a coexistence of ferroelectric (Curie temperature, T_c of 830 °C) [2, 3] and

✉ Nikolina Pavlovic
nikolina.pavlovic@uhasselt.be

Jan D'Haen
jan.dhaen@uhasselt.be

Hiwa Modarresi
hiwa.modarresi@fys.kuleuven.be

Alexander Riskin
alexander.riskin@uhasselt.be

Christopher De Dobbelaere
christopher.dedobbelaere@uhasselt.be

Margriet J. Van Bael
margriet.vanbael@fys.kuleuven.be

Kristiaan Temst
kristiaan.temst@fys.kuleuven.be

An Hardy
an.hardy@uhasselt.be

Marlies K. Van Bael
marlies.vanbael@uhasselt.be

1 Inorganic and Physical Chemistry and IMEC Division IMOMEC, Institute for Materials Research, Hasselt University, Martelarenlaan 42, 3500 Hasselt, Belgium

2 Materials Physics, Institute for Materials Research, Hasselt University, Wetenschapspark 1, 3590 Diepenbeek, Belgium

3 Instituut voor Kern-en Stralingsfysica, KU Leuven, Celestijnenlaan 200D, 3001 Leuven, Belgium

4 Laboratorium voor Vaste-Stoffysica en Magnetisme, KU Leuven, Celestijnenlaan 200D, 3001 Leuven, Belgium

magnetic (Néel temperature, T_N of 370 °C) [3, 4] functionalities at room temperature. However, secondary phases like mullite-type $Bi_2Fe_4O_9$ and sillenite-type $Bi_{25}FeO_{39}$ usually accompany BFO [5–8]. The presence of such parasitic phases in the material can deteriorate electrical and magnetic properties, diminishing application possibilities and performances [9]. Although a lot of research has been carried out on the BFO system and issues with secondary phases are often reported, the various literature reports dealing with the thermal stability of BFO and the reasons for the appearance of these parasitic phases are still contradictory [5–8, 10–14].

Early works on the solid-state synthesis of BFO suggest that its decomposition into the starting oxides Bi_2O_3 and Fe_2O_3 [10] or $Bi_2Fe_4O_9$ [5] during thermal treatment is the consequence of the evaporation of bismuth oxide [5, 10]. In more recent papers, difficulty to obtain a single-phase material is attributed to the changing equilibrium composition of BFO upon temperature increase by Morozov et al. [8], while Palai et al. [12] emphasize that the $BiFeO_3$ phase is thermodynamically metastable in air. The latter authors [12] as well as Arnold et al. [2] report decomposition around 820 °C into an iron-rich $Bi_2Fe_4O_9$ and a liquid phase suggesting that the rate of decomposition can be affected by several different parameters including the ratio of surface to bulk volume, the annealing time at constant temperature, heating rate, surface defects, porosity and grain size, etc. During neutron diffraction measurements, Palewicz et al. [4] noticed that part of the BFO sample transformed to the new $Bi_2Fe_4O_9$ phase at 700 °C. In their comprehensive study of BFO phase stability, Valant et al. [7] pointed out that the purity of the starting materials is a crucial parameter for obtaining single-phase BFO since the presence of small amounts of impurities leads to the formation of a significant amount of secondary phases. According to the latter, Al_2O_3 or SiO_2 impurities enhance the formation of secondary phases during solid-state synthesis, since Al_2O_3 and SiO_2 have a higher solubility in $Bi_2Fe_4O_9$ and $Bi_{25}FeO_{39}$, respectively, than in $BiFeO_3$. Selbach et al. [6] report that $BiFeO_3$ decomposes into $Bi_{25}FeO_{39}$ and $Bi_2Fe_4O_9$ in a temperature interval from 450 to 770 °C under ambient atmosphere while above this interval till 930 °C $BiFeO_3$ is thermodynamically stable and corroborate their findings with thermodynamic explanations. Decomposition at temperatures higher than 770 °C is therefore related to chemical incompatibility between $BiFeO_3$ and the supporting materials it is in contact with during processing, like Al_2O_3- or SiO_2-based substrates [11]. In this case, alumina or silicon substrate at the contact surface with BFO sample can act like impurities [7] initiating an interface reaction which results in a higher amount of Bi-rich and Fe-rich secondary phases in $BiFeO_3$ ceramics [11] as evidenced during some experimental studies [15, 16].

The aforementioned studies have mainly focused on the conventional solid-state synthesis, as a method for the preparation of single crystals, powders, and ceramics. However, the different processing conditions between bulk ceramics and thin films could cause differences in phase stability, decomposition behavior, and formation of secondary phases. Furthermore, synthesis parameters known to influence the phase formation and stability of the material differ between preparation methods and state of matter. Therefore, here we study thin films.

Deposition of BFO thin films is achievable via numerous methods including both physical vacuum-based techniques such as pulsed laser deposition (PLD) [12, 17, 18], molecular beam epitaxy (MBE) [19], or sputtering [20–22] and chemical-based techniques such as chemical vapor deposition (CVD) [23], sol–gel or chemical solution deposition (CSD) [24–29], or electrophoretic deposition [30]. Previous reports on the phase stability of the BFO thin films mainly refer to PLD processing conditions where deposition pressure and temperature play an important role in the phase formation process while issues with impurities like Fe_2O_3 and Bi_2O_3, as well as Bi evaporation were reported [9, 18, 31, 32]. On the other hand, research on the thermal stability of BFO thin films obtained via CSD and on the influence of processing parameters is rather limited [27, 28]. Particularly in solution chemistry, the thermal budget (pyrolysis and annealing times and temperatures, heating rates) and possible film–substrate interactions are important aspects of solution deposition [27, 28, 33, 34].

In this paper, we report on the thermal stability and the decomposition of BFO thin films obtained via water-based CSD. We identified processing parameters affecting the decomposition of $BiFeO_3$, which is followed by a thorough microstructural analysis of the acquired thin films and the determination of the phases present. We also propose approaches to inhibit the formation of secondary phases and improve the stability of the BFO phase.

Experimental

Solution preparation

Bismuth ferrite thin films were deposited from an aqueous solution–gel precursor on platinized silicon substrates with TiO_x as an adhesion layer between the Pt electrode and the silicon substrate (Pt (80 nm)/TiO_x (30 nm)/SiO_2/Si). First, we synthesized aqueous solutions of bismuth and iron complexes with citric acid as the chelating agent. More details on the synthesis of these precursor solutions can be found elsewhere [35]. The exact concentration of the metal ion in the monometal precursors was determined by means of ICP–AES (Optima 3300 DV, PerkinElmer). Then, by mixing the Bi^{3+} and Fe^{3+} solutions in the stoichiometric ratio as well as with a Bi excess of 10, 20, or 30 mol%, we obtained multi-metal ion precursor solutions with a total metal ion concentration of 0.6 M. Besides these BFO precursors, we also prepared solutions where the Fe^{3+} ion was partially substituted by Ti^{4+} and without Bi excess. The source for Ti^{4+} was an aqueous-citrato-peroxo-Ti(IV) precursor of which the synthesis route was reported earlier [36]. In this way, we obtained four different solutions as precursors for $BiFe_{1-x}Ti_xO_3$ (BFTO) with a total metal ion concentration of 0.6 M, in which $x = 0.05$, 0.10, 0.15, or 0.20.

Thin film deposition

All solutions were filtered through a syringe filter of 0.2 μm (Acrodisc Premium, Pall Life Sciences) for their deposition onto platinized silicon substrates (Pt/TiO_x/SiO_2/Si) which were thoroughly cleaned beforehand in sulfuric acid peroxide mixture/ammonia peroxide mixture (SPM/APM) to improve their wettability [37]. Thin layers were spin coated at a rotation speed of 3000 rpm for 30 s, with an acceleration of 1000 rpm/s. Each deposition step was followed by a hot plate treatment at 110 °C (1 min), 260 °C (2 min), and 480 °C (2 min) in order to decompose the organic constituents. The thickness of the obtained films is controlled by the number of deposited layers. Finally, the films were subjected to an annealing process by inserting them into a preheated tube furnace at 600, 650, or 700 °C for different times in a dry air atmosphere using a gas flow of 0.5 l/min.

Characterization

The crystal structure of the obtained films was analyzed using a Siemens D-5000 diffractometer with Cu $K_{\alpha 1}$ radiation operating in θ–2θ mode with 2θ range from 10° to 60°. Film morphology and microstructure were examined using an atomic force microscope (Veeco Dimension Microscope AFM with Digital Instrument Nanoscope III controller), scanning electron microscope (SEM, FEI Quanta 200 FEG) coupled with energy-dispersive X-ray spectroscopy (EDX) analysis, and electron backscattered diffraction (EBSD) analysis. For the phase analysis, the SEM images were taken under EBSD conditions i.e.. the sample was tilted ~70° with respect to the horizontal axis, which allows more electrons to be scattered and to escape toward the detector. The thickness of the annealed films is measured in cross-sectional view with a scanning electron microscope (SEM) which revealed that film thickness shows a linear dependence on the number of deposited layers. Magnetic response of the samples was measured by superconducting quantum interface device (SQUID) magnetometer of Quantum Design MPMSXL-5 with a reciprocating sample option (RSO) head at 300 K with the magnetic field in plane with the thin films.

Results and discussion

Annealing temperature

X-ray diffraction (XRD) analysis reveals that $BiFeO_3$ films already crystallize around 470 °C after a short thermal treatment of 2 min, as shown in Fig. 1a. This result is in agreement with Tyholdt et al. who reported the crystallization of 2-methoxyethanol-based BFO films between 460 and 480 °C [28]. The fact that crystallization from solution-based precursors already starts at a lower temperature, in comparison with solid-state methods (~600 °C) [10] is intrinsically ascribed to the wet chemical method enhancing the mixing of metal ions at the molecular level, thereby decreasing diffusion distances and facilitating a low crystallization temperature [38].

In order to get insights into phase formation, growth, and thermal stability of the stoichiometric BFO films, three-layered films were further annealed at 600, 650, or 700 °C for 1 h in dry air. XRD results shown in Fig. 1b confirm that the BFO phase is present in all three films treated under these different thermal conditions. Films annealed at 600 °C crystallized into the BFO phase without any other secondary phase detectable within the instrumental sensitivity. An increase of temperature by 50 °C did not introduce significant differences in the pattern.

Drastic changes in phase composition occurred after heat treatment at 700 °C: a large portion of the iron-rich $Bi_2Fe_4O_9$ has formed as a secondary phase. Furthermore, besides the phases detected above, additional peaks at $2\theta \approx 27.9°$ and $\approx 30°$ appearing as shoulders to the main reflections of $Bi_2Fe_4O_9$ ($2\theta = 28.21°$ and 29.7°), as well as a peak at $2\theta \approx 34.8°$ point to the presence of other secondary phases in the films. Of these, the first two reflections could be correlated to a bismuth-rich Bi_2O_3 or $Bi_{25}FeO_{39}$ phase. However, the reflection around 30° could also have its origin in some form of a Pt–Bi alloy, Pt–Bi–O compound, or even in a $Bi_2Ti_2O_7$ phase together with the peak at $2\theta \approx 34.8°$ (marked with ?) [33, 39]. Figure 2 illustrates the effect of the annealing temperature on the film morphology. The film annealed at 600 °C is polycrystalline with equiaxial grains, uniform, relatively smooth, with a low porosity, and without cracks. However, after thermal treatment at 650 °C, the SEM images reveal dark areas having a different morphology compared to the rest of the film which can probably be related to the onset

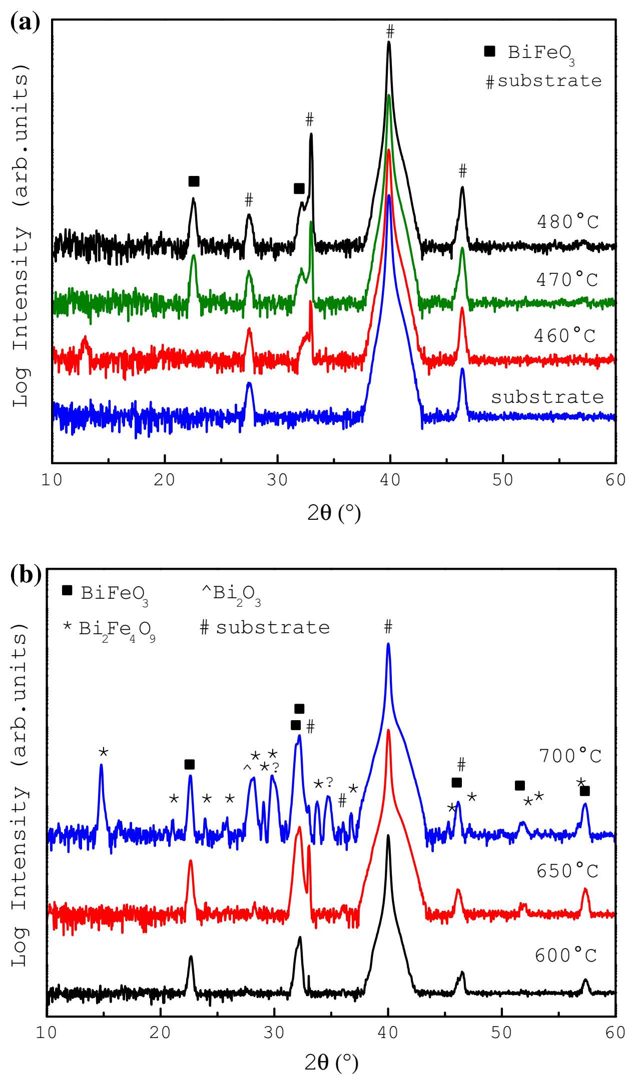

Fig. 1 XRD patterns of the three-layered films **a** after a hot plate treatment at 460, 470, or 480 °C for 2 min and **b** annealed at 600, 650, or 700 °C for 1 h in dry air

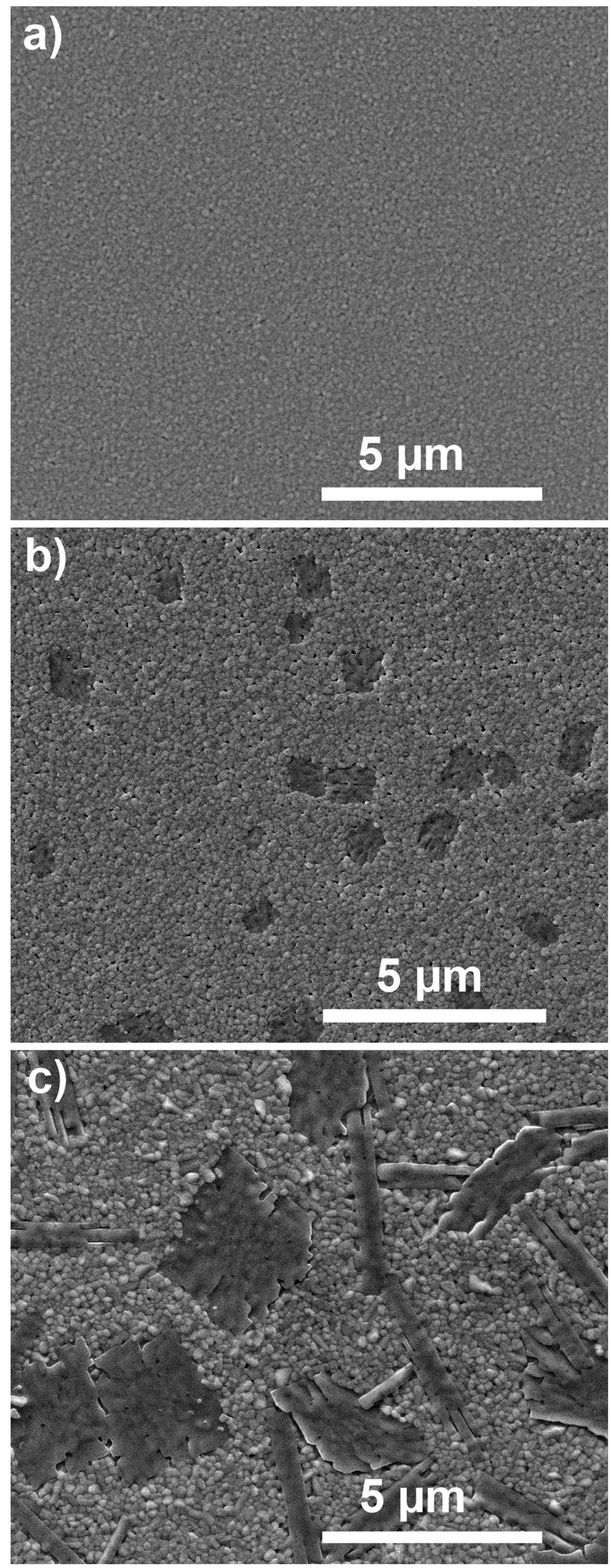

Fig. 2 SEM images of the stoichiometric three-layered films annealed at **a** 600 °C, **b** 650 °C, or **c** 700 °C for 1 h

of the BFO decomposition process. The morphological change is the most drastic in the sample annealed at 700 °C, where large, elongated grains of around 5 µm are embedded in the matrix of small, equiaxed grains. According to EDX analysis (not shown), these elongated grains comprise a higher amount of Fe compared with the amount that is found in the surrounding matrix.

Electron backscattered diffraction is used in conjunction with SEM imaging to perform a qualitative microstructural analysis of the films annealed at 700 °C, as shown in Fig. 3a–c. According to the Kikuchi pattern (Fig. 3b) obtained from the matrix (position 1), this part of the film is identified as $BiFeO_3$, while the patterns from the big, elongated grains (position 2 and 3) correspond to iron-rich

$Bi_2Fe_4O_9$ (Fig. 3c). The phase map in Fig. 3d shows the BFO grains in red and the $Bi_2Fe_4O_9$ in blue. Inverse pole figure (IPF) maps for each phase separately are in reference to the normal direction where each individual orientation of crystals is colored differently. Color coding for the orientations is presented in a standard stereographic triangle (SST) [40], in Fig. 3e–f. The small grains are randomly oriented indicating the polycrystalline nature of the BFO film while the large grains of $Bi_2Fe_4O_9$ are single crystals that mainly exhibit (001) orientation (red–orange color in the SST). Despite this thorough microstructure analysis, there is no evidence of Bi-rich phases although bismuth-rich compounds are detected by XRD analysis as one of the formed phases during the decomposition process (Fig. 1b). Furthermore, the detection limit of the diffraction analysis for Bi-rich phases should be lower since the concentration of heavy Bi ions is much higher in Bi_2O_3 or $Bi_{25}FeO_{39}$ than in compounds with the lighter Fe ion, such as $Bi_2Fe_4O_9$. It is possible that the Bi-rich phase is spread in the films as very fine grains or is segregated as a separate layer below the film, on the interface with the substrate [41].

According to several reports where Bi-based films were deposited on substrates with a Pt bottom electrode, diffusion of Bi from the film into the substrate and its interaction with the platinum electrode result in the formation of an interfacial layer at the electrode–film interface [29, 39]. It is known that Bi reacts with Pt forming very stable intermetallic compounds [42], thus an interdiffusion layer between a Bi-based film and a Pt electrode can readily form at elevated temperatures [29, 33, 39]. A similar phenomenon was observed in case of Pb-based thin films obtained by CSD where different Pt–Pb intermetallic phases formed at elevated temperature [43, 44].

Based on the SEM and EBSD results in Figs. 2 and 3, respectively, it can be assumed that the decomposition process already starts at 650 °C, where the dark areas in the SEM images (Fig. 2b) are sites where nucleation of the iron-rich $Bi_2Fe_4O_9$ phase starts and from where its large grains develop at 700 °C. In order to get insight into and possibly extend the stability window of the BFO films toward 700 °C, several experiments are performed taking into consideration the film thickness, annealing time, Bi excess, and usage of an aliovalent substituent as parameters that could influence the phase stability of the obtained films.

Film thickness

Due to the specific geometry of thin films i.e., their high surface-to-volume ratio and large exposed surface area, bismuth oxide, being a volatile compound, can evaporate much easier from a thin film than from bulk material during heat treatment. According to the phase diagram of $BiFeO_3$, a Bi deficiency in the material could lead to the destabilization of the $BiFeO_3$

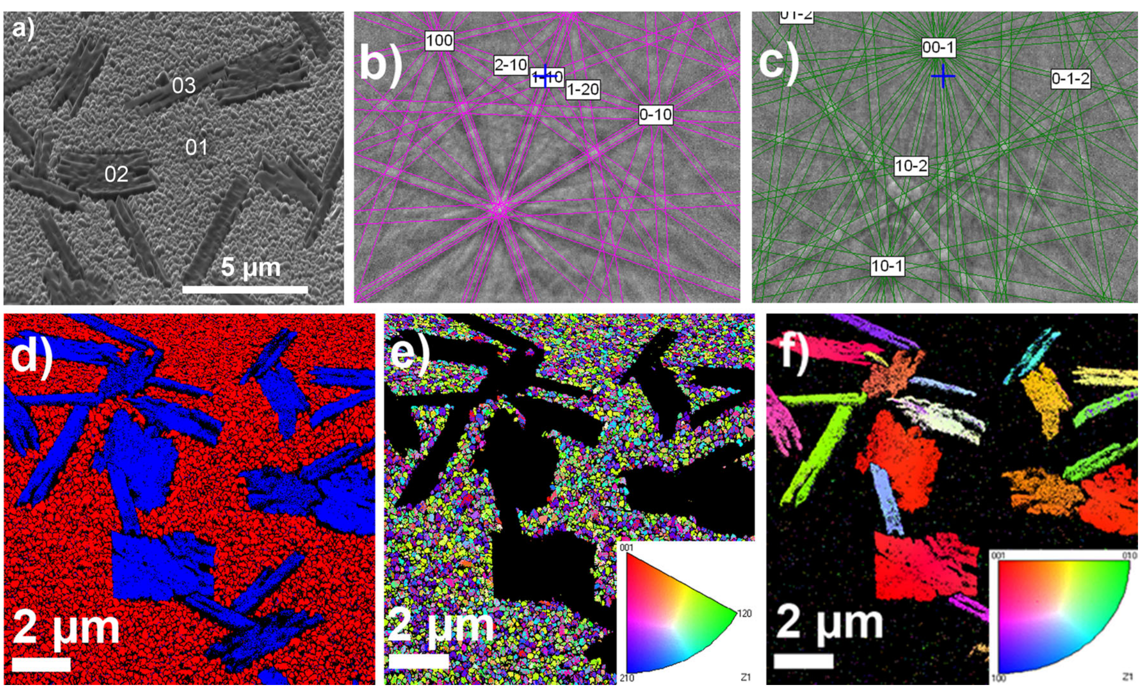

Fig. 3 EBSD results of the three-layered BFO film annealed at 700 °C: **a** SEM image of the sample, **b** Kikuchi pattern obtained at position 01: $BiFeO_3$, **c** Kikuchi pattern obtained at position 02: $Bi_2Fe_4O_9$; **d** phase map (*red*: $BiFeO_3$, *blue*: $Bi_2Fe_4O_9$), **e** and **f** are inverse pole figure (IPF) maps for the $BiFeO_3$ and $BiFe_2O_4$ phase, respectively, in reference to normal direction with the color codes for individual orientations of crystals presented in standard stereographic triangle (SST) (Color figure online)

phase and the formation of iron-rich $Bi_2Fe_4O_9$ [12]. By changing the film thickness, the ratio of surface to volume is varied in order to explore its influence on the phase stability of BFO. For this study, one-, three-, six- and eight-layered films were deposited, annealed at 700 °C for 1 h, and mutually compared. XRD patterns presented in Fig. 4a show that regardless of the film thickness, substantial amounts of secondary phases form. However, the most drastic change in phase composition occurs in the one-layered films, where $Bi_2Fe_4O_9$ appears as the primary phase with a preferred orientation of (001). At the same time, the decomposition is not complete since a few peaks of BFO are still present. Reflections at $2\theta \approx 27.9°$ corresponding to a Bi-rich phase are only visible for the thicker films, while reflections from a possible Pt–Bi alloy are detected at a $2\theta \approx 30°$, marked with (?) in Fig. 4b.

A thicker film slightly stabilizes the BFO phase but also has a large impact on the morphology, as illustrated in Fig. 5. The SEM micrograph of the one-layered film reveals a broken-up layer consisting of small, equiaxed grains, and larger structures differing in shape and size which could be associated with the decomposition process and the formation of $Bi_2Fe_4O_9$. Such a heterogeneous morphology is in agreement with the XRD results (Fig. 4). The secondary phase is also present in the microstructure of the six-layered samples in the form of plate-like grains roughly square in shape with an edge length up to 1 µm. In the case of eight-layered films, smaller and thicker plates of the iron-rich phase are embedded in the BFO matrix. In general, well-defined $Bi_2Fe_4O_9$ grains of different morphologies are formed with a tendency toward a decreasing grain size with an increase of film thickness. Besides, the increasing thickness results in a gradual change of (001) preferred orientation of $Bi_2Fe_4O_9$ in one-layered films to more randomly oriented grains after deposition of 8 layers. In the cross-sectional SEM images of the six- and eight-layered films in Fig. 5, one observes that single-crystalline grains of the iron-rich phase grow through the whole film and are not only present on the film surface. Nucleation of these $Bi_2Fe_4O_9$ grains probably occurs at the film/substrate interface, after which grain growth continues toward the film surface through the depletion of the BFO phase. According to literature, $Bi_2Fe_4O_9$ crystals have a variable morphology and can be either sheet, plate, cube, rod, or fiber like depending on the processing parameters during the synthesis [45–49]. The possible explanation for this variety of crystal shapes can be found in the crystal structure of $Bi_2Fe_4O_9$ [45, 50]. Previous studies on orthorhombic $Bi_2Fe_4O_9$ showed that the dominating facets of $Bi_2Fe_4O_9$ crystal are (001), (110), and $(\bar{1}10)$. Crystal growth occurs easily along the (001) plane, resulting in a sheet-like morphology with a large (001) facet. If the growth on (110) and $(\bar{1}10)$ facets is suppressed and

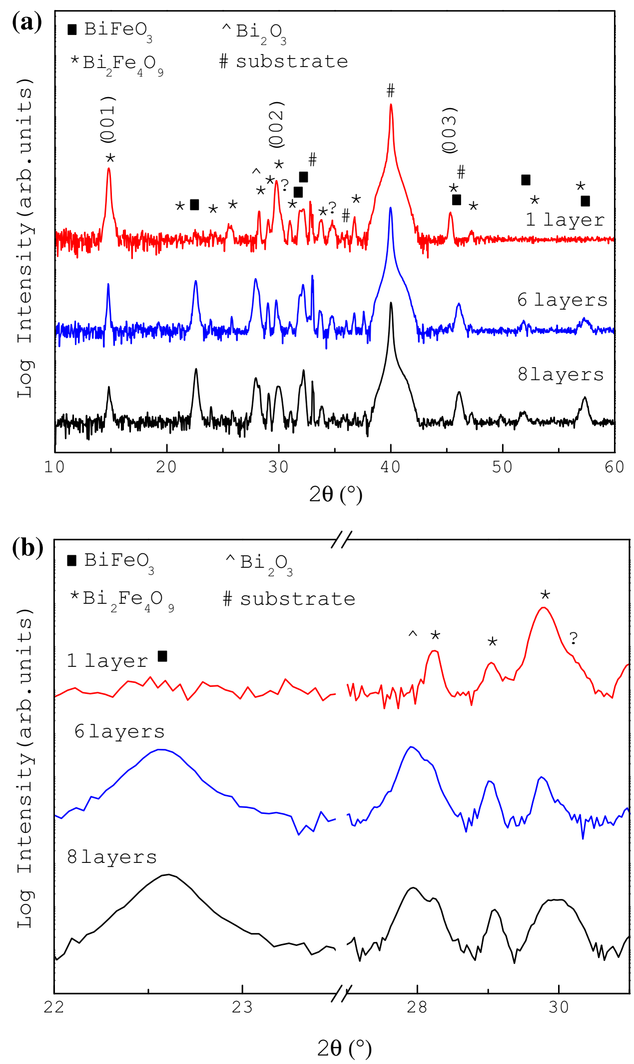

Fig. 4 **a** XRD patterns of BFO films obtained from one, six, and eight layers, annealed at 700 °C; **b** Detail from the diffractograms in (**a**)

enhanced on the (001) facet, the growth rate difference between these facets decreases or disappears. As a result, the morphology of the $Bi_2Fe_4O_9$ crystal changes to a plate like or to a cubic form.

In the same images, the interface between the Pt and the TiO_x adhesion layer beneath it can be studied. The thicknesses of the platinum and TiO_x layers vary locally along the sample. Furthermore, the interface between Pt and TiO_x is very rough in comparison with the bare $Pt/TiO_x/SiO_2/Si$ substrate itself (Fig. 5f), which could be the result of possible interactions of these layers with the BFO film, the formation of a Pt–Bi alloy, or even the accumulation of Bi beneath the platinum layer. To draw more conclusions from the interaction between Bi and the Pt substrate at elevated temperatures, we deposited an aqueous Bi citrate

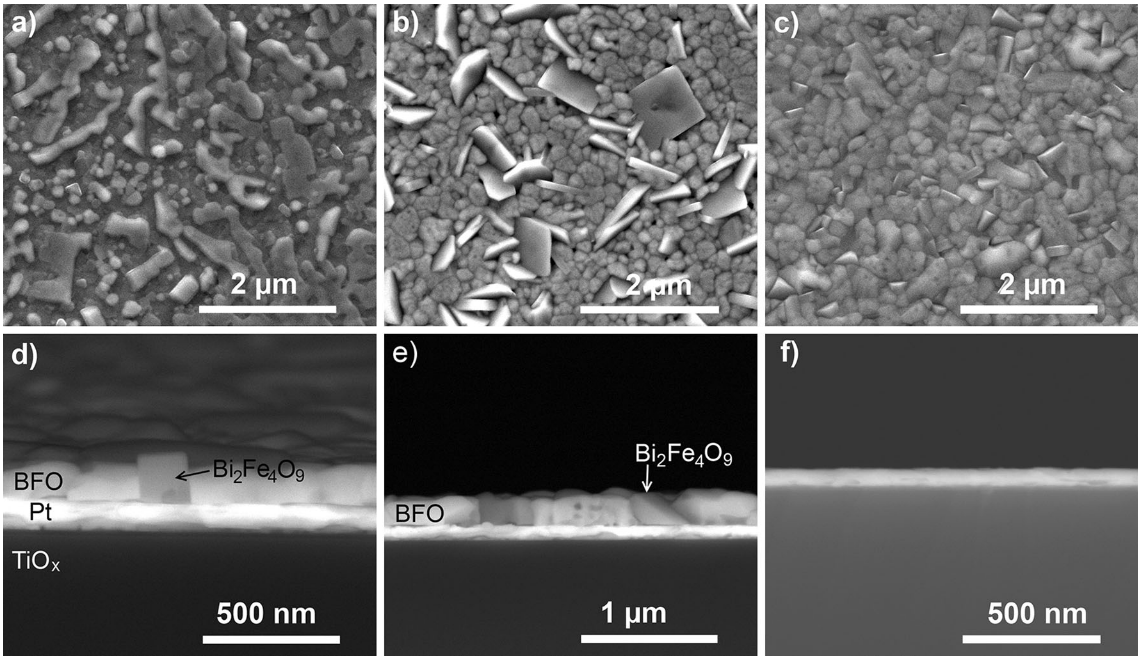

Fig. 5 SEM surface images of BFO films annealed at 700 °C with **a** one, **b** six, or **c** eight layers; Backscattered electron images of cross section of **d** six- or **e** eight-layered films and **f** the Pt/TiO_x/SiO_2/Si substrate treated at 700 °C

precursor with a 0.7 M concentration on the same substrate and repeated the same thermal treatment with the final annealing at 700 °C for 1 h. An SEM micrograph of the obtained film and a backscattered electron image of the cross section are given in Fig. 6. A broken layer with island-shaped structures of bismuth oxide and open, crater-like features on the Pt electrode are clearly visible in the plane-view SEM image, Fig. 6a. These features indicate the strong interaction between the Pt electrode and the film and probably appear due to severe diffusion of bismuth through the electrode and its accumulation beneath the platinum, as shown in the cross-sectional image in Fig. 6b.

Annealing time

To study the influence of the annealing time on the decomposition process, we exposed the stoichiometric, three-layered $BiFeO_3$ films to 700 °C for different times (5, 10, 30, 60, 90, or 120 min) and afterward analyzed the phase composition by X-ray diffraction. As Fig. 7a shows, only a small amount of the $Bi_2Fe_4O_9$ secondary phase is present in the film after 10 min of heat treatment. With longer annealing times, the intensities of the $Bi_2Fe_4O_9$ (001) and (002) reflections at $2\theta = 14.7°$ and 29.7°, respectively, show the most prominent increase. In addition to $Bi_2Fe_4O_9$, as a product of the BFO decomposition process, other secondary phases are also present in the samples as shown by the peaks in the 2θ range 20°–34° in Fig. 7b. A closer examination of this pattern shows double peaks at $2\theta \approx 28°$, as well as a shoulder at $\approx 30°$ which probably arise from Bi-rich phases and the Pt–Bi alloy, respectively, as discussed above. As the annealing time increases, the integral intensities of the BFO reflections decrease while the ones belonging to the iron-rich $Bi_2Fe_4O_9$ phase increase. According to these results, longer annealing times at 700 °C enhance the decomposition process and thus the formation of secondary phases in the BFO films, as expected.

The SEM images in Fig. 8 show the evolution of the film morphology with respect to the annealing time. Some microstructural diversity appears already after exposure at 700 °C for 10 min in the form of longer grains. As time increases, it is clearly visible how big elongated grains of $Bi_2Fe_4O_9$ gradually expand in between the small grains of the BFO matrix.

Addition of Bi excess

Considering Bi evaporation from the film as a cause for the secondary phase formation, a bismuth excess in the precursor is a possible step to prevent the decomposition of BFO [28, 51, 52]. According to Tyholdt et al., a bismuth excess of 10 at.% Bi improves not only the stability of the BFO phase at elevated temperatures (700 °C) but also the quality of the films in terms of density and porosity [28]. In our study, a significant amount of $Bi_2Fe_4O_9$ is present in the three-layered films with a 10 mol% Bi excess, as in Fig. 9. On the other hand, by applying 20 or 30 mol% Bi

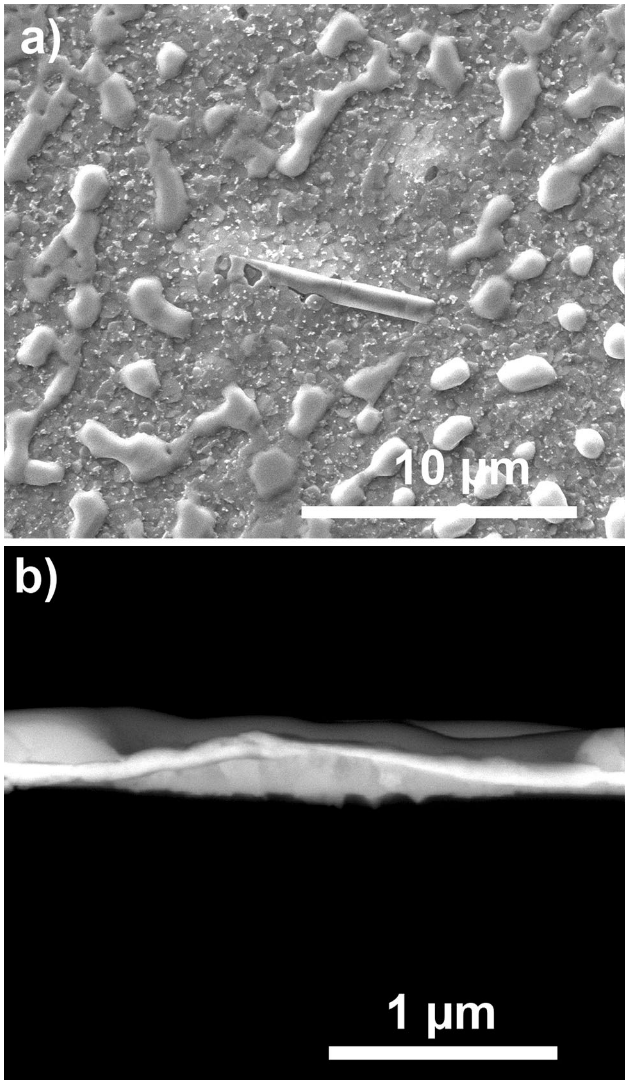

Fig. 6 Film obtained from a Bi citrate precursor (0.7 M) deposited on Pt/TiO_x/SiO_2/Si using the same thermal treatment at 700 °C/1 h as for the BFO films: **a** Plane-view SEM micrograph, **b** Cross-sectional backscattered image where the very bright layer is Pt electrode and dark area underneath is Bi-rich phase

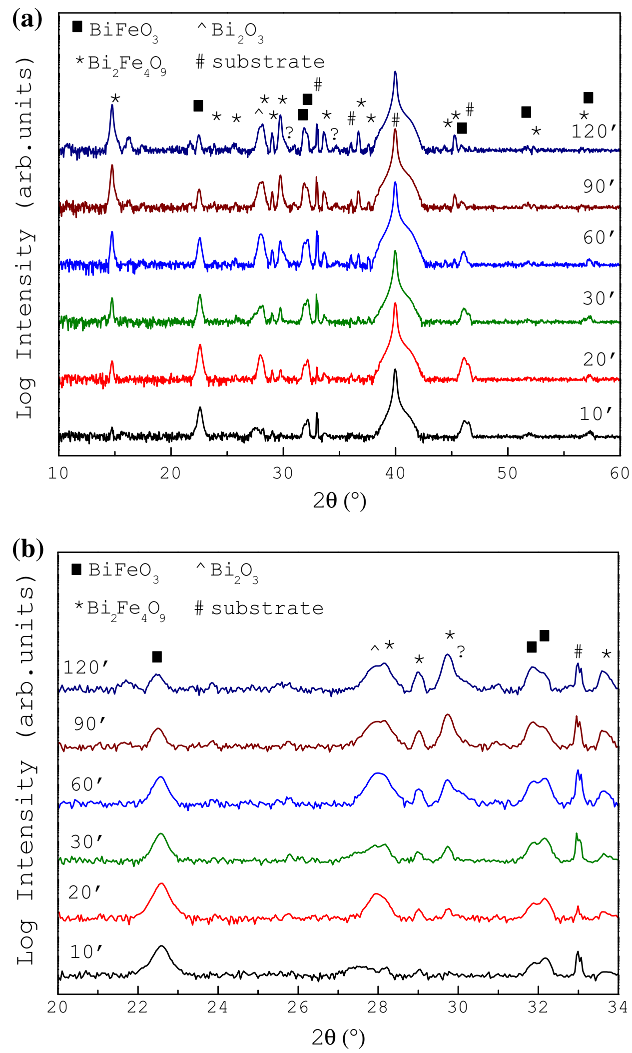

Fig. 7 **a** XRD patterns of three-layered BFO films annealed at 700 °C for different times (10, 20, 30, 60, 90, or 120 min); **b** Detail from the diffractogram in (**a**)

excess in the precursor solutions, it is possible to suppress, at 700 °C, the formation of the iron-rich phase of which reflections are no longer detected in the XRD patterns after heat treatment, as shown in Fig. 9. However, peaks of other secondary phases, probably a Bi-rich phase and some form of Pt–Bi alloy (marked with ?), are still detected. The film with a 10 % Bi excess has a very heterogeneous microstructure due to the decomposition leading to the formation of the iron-rich secondary phase, as shown in Fig. 10a. Figure 10b and c shows a remarkable improvement of the microstructural homogeneity which is in accordance with the XRD results. In case of the films with 20 and 30 mol% Bi excess, the SEM images reveal more dense microstructures, although a few square-shaped grains, rich in iron, are still visible in films with a 20 mol% Bi excess.

Substitution of Fe with Ti

Chemical substitution into perovskite BFO has mainly been used to improve electrical and magnetic properties of the material [53–58]. The substitution of Fe^{3+} by aliovalent Ti^{4+} results in a reduced leakage current. It is reported that titanium with a higher valence Ti^{4+} ion than Fe^{3+} acts as a donor decreasing the concentration of oxygen vacancies [24, 25, 53, 59]. In our work, the effect of the addition of different amounts of Ti on the phase stability of BFO films ($BiFe_{1-x}Ti_xO_3$, $x = 0.05$, 0.1, 0.15 or 0.20) is studied. Noteworthy changes in the XRD patterns are visible as the amount of Ti increases, as shown in Fig. 11. Reflections

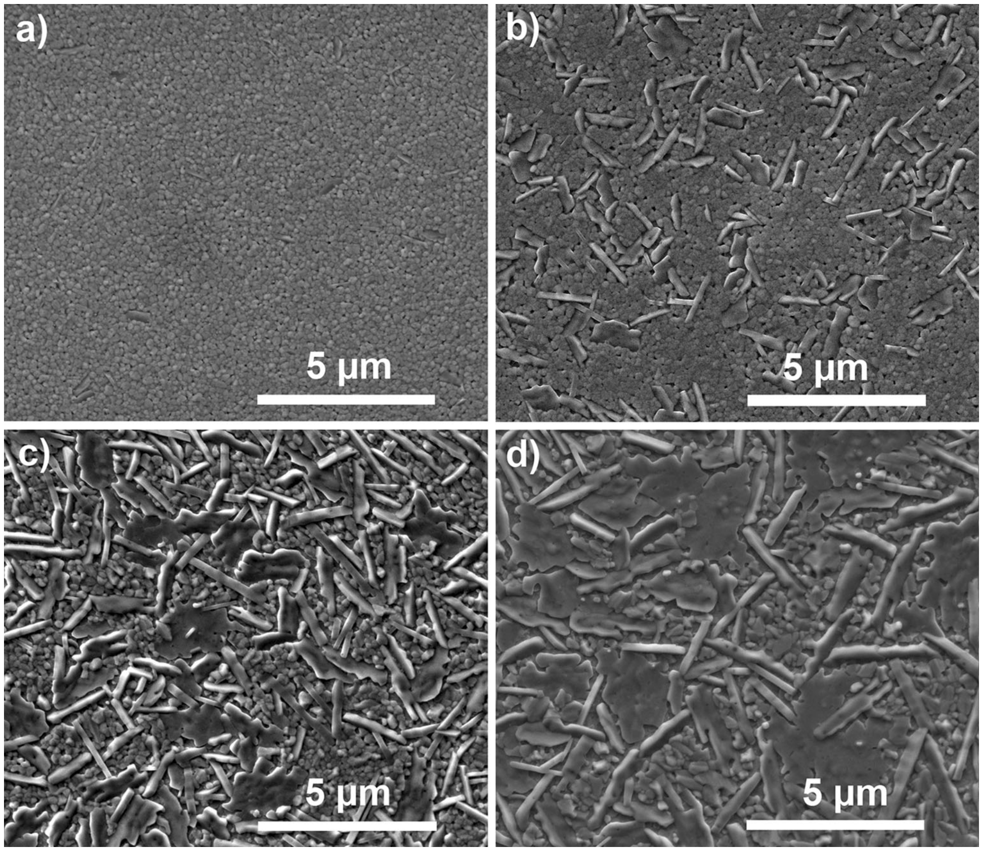

Fig. 8 SEM images presenting the evolution of the film morphology with annealing time at 700 °C: **a** 10, **b** 30, **c** 90, or **d** 120 min

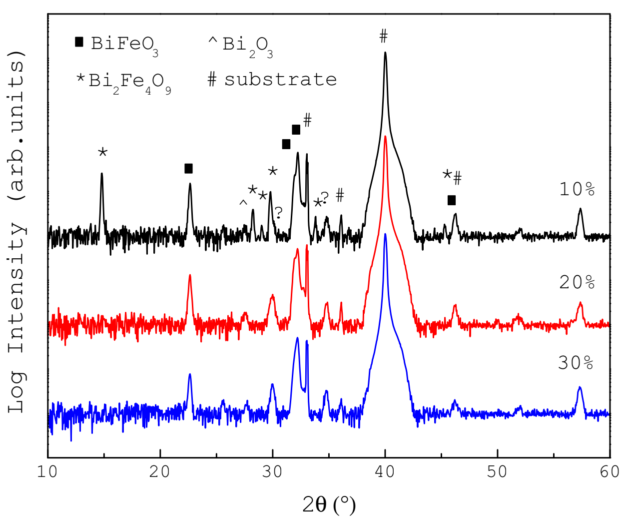

Fig. 9 XRD patterns of three-layered films with a different Bi excess annealed at 700 °C/1 h

belonging to an iron-rich phase become less pronounced which implies that the presence of the Ti^{4+} ion in the system partially stabilizes the BFO phase. The most prominent change is the complete disappearance of $Bi_2Fe_4O_9$ as a result of substitution with 20 mol% Ti. At the same time, with an increase of the Ti content toward $x = 0.20$, the peak at $2\theta \sim 32°$ associated with BFO becomes more broadened. This peak broadening is connected with a decreasing average grain size below 100 nm, as shown in Fig. 12e. SEM images reveal a slightly higher porosity in the Ti-substituted films. Furthermore, the growth rate of the large iron-rich grains of the secondary phase at 700 °C is significantly lower as the amount of Ti increases. Elongated grains of ~5 µm, appearing in the unsubstituted films, decrease to below 1 µm and finally disappear in those samples with the highest Ti concentration.

Similar effects of Ti substitution on the growth of $BiFeO_3$ grains in bulk ceramics and thin films were found by several authors [60–64]. Bernardo et al. observed a positive effect of Ti substitution on the phase stabilization of BFO ceramics for classical solid-state synthesis [60, 61]. The partial stabilization of BFO and the inhibition of grain growth are probably results of two phenomena: entering of Ti^{4+} ions inside the perovskite structure and segregation of Ti due to limited incorporation. As mentioned before, Ti^{4+} ions in the structure behave as a donor and thus can suppress the formation of oxygen vacancies which in turn

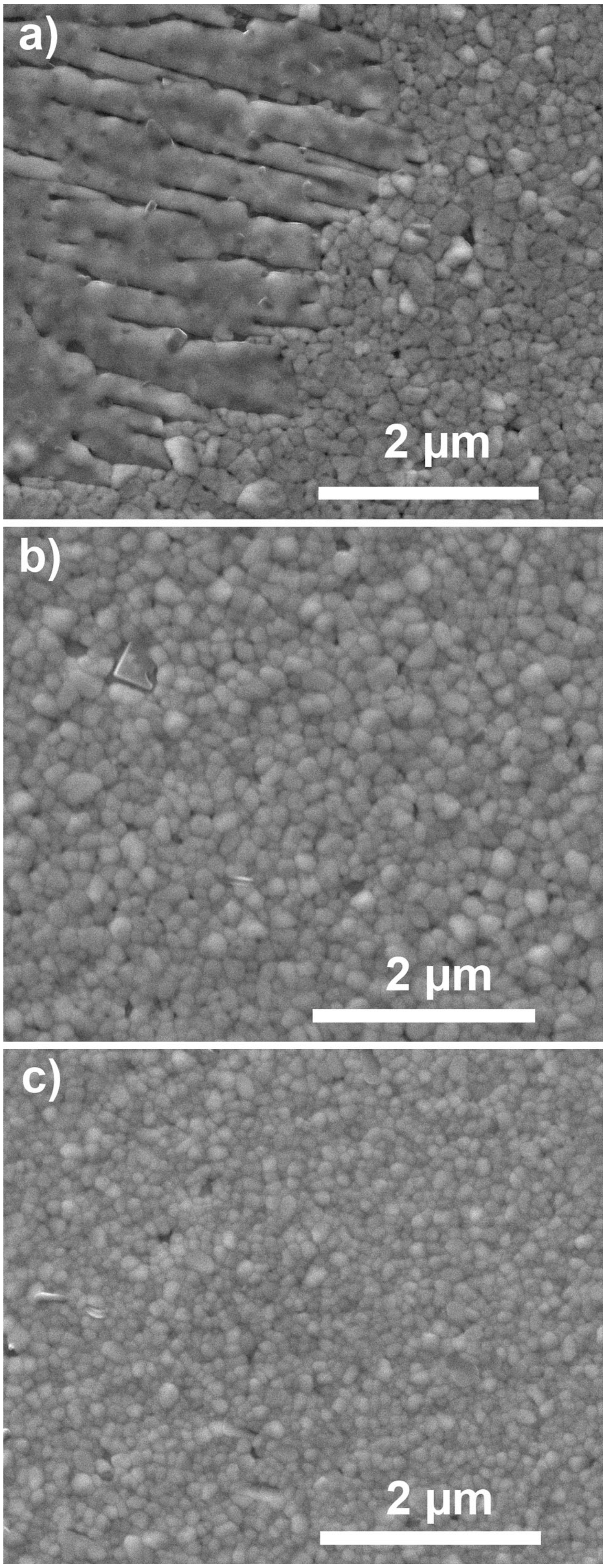

Fig. 10 SEM micrographs of three-layered films with **a** 10 %, **b** 20 %, or **c** 30 % Bi excess annealed at 700 °C/1 h

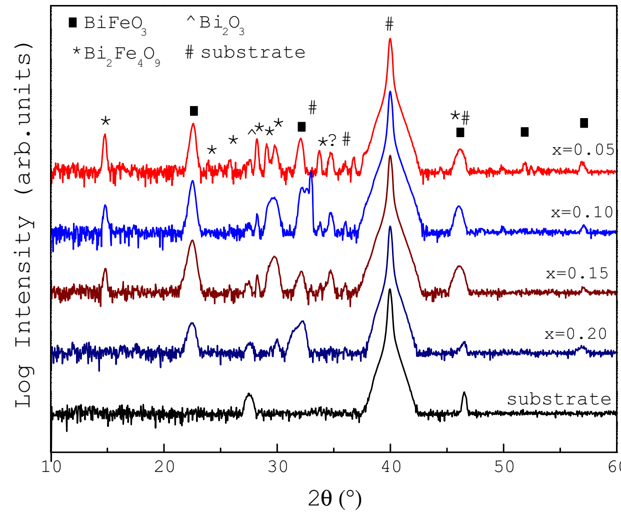

Fig. 11 XRD patterns of $BiFe_{1-x}Ti_xO_3$, ($x = 0.05$, 0.10, 0.15 or 0.20) films annealed at 700 °C/1 h

limits the diffusion of matter resulting in a lower rate of grain growth [60, 63, 65]. Moreover, in a recent paper, Bernardo and coauthors reported thorough microstructural analyses of Ti-doped ceramics [61]. Interestingly, they found clusters of nanometer-sized grains separated by Ti-rich layers. Due to the segregation of Ti from the structure, the Ti-rich areas are formed at the inner grain boundaries where they hinder the grain boundary mobility inhibiting the growth of grains. In ceramic processing, this type of grain growth control is known as the solute drag-based mechanism [61].

Discussion on thermal stability of BFO films

The observed decomposition onset of BFO films in this work at 650 °C is consistent with the BFO temperature metastable range around 450–770 °C reported by Selbach et al. for BFO bulk ceramics [6]. The partial decomposition of the BFO phase into Bi-rich and Fe-rich phases in this temperature range can be explained by the more thermodynamically stable secondary phases in comparison to the BFO phase [6]. Further evidence of the instability of the BFO phase is the fact that decomposition is enhanced by increasing the annealing temperature to 700 °C as well as lengthening the annealing time. The observed influence of these parameters on phase stability is in agreement with the reports where the rate of BFO decomposition is determined by processing temperature [2, 12] or extended annealing time [8, 12]. Furthermore, detection of large $Bi_2Fe_4O_9$ grains by SEM and EBSD in this study suggests a Bi deficiency occurring in the films during processing. In case of BFO ceramic, large $Bi_2Fe_4O_9$ grains observed at temperatures as high as 880 °C

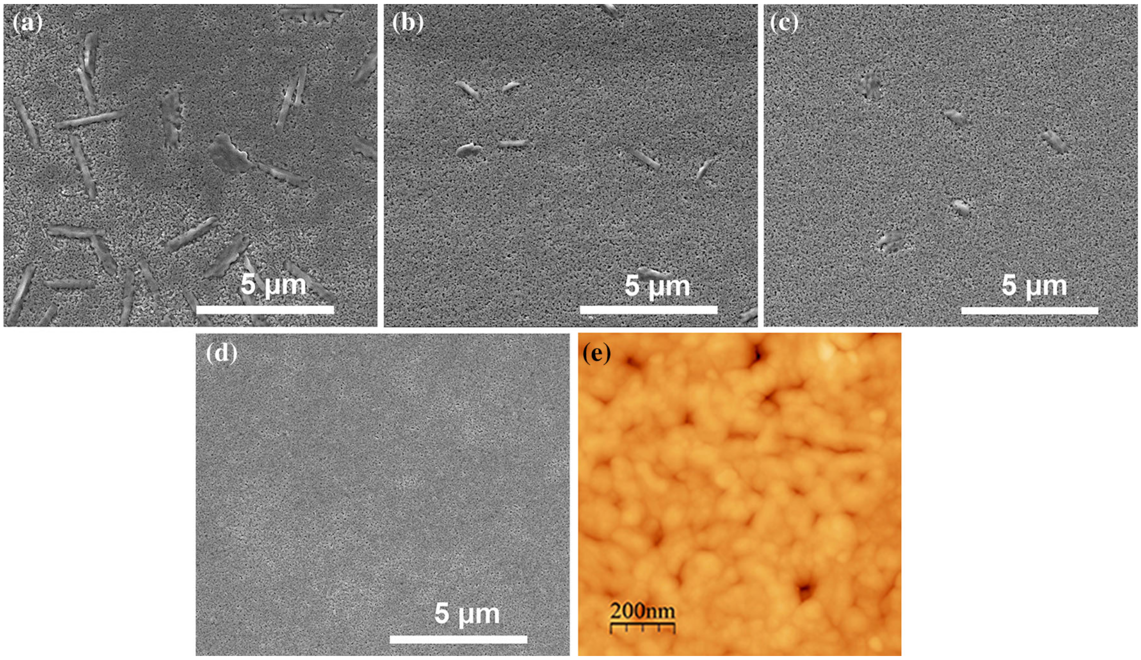

Fig. 12 SEM micrographs of $BiFe_{1-x}Ti_xO_3$ films annealed at 700 °C/1 h with **a** $x = 0.05$, **b** 0.10, **c** 0.15, **d** 0.20, and **e** AFM image of $BiFe_{0.85}Ti_{0.15}O_3$ film

are related to Bi_2O_3 loss due to evaporation during sintering [16] and are different from the $Bi_2Fe_4O_9$ grains that appear together with Bi-rich grains due to diffusion limitations during solid-state synthesis [14, 66]. However, for the films studied here, the Bi_2O_3 deficiency is probably conditioned by the specific thin film geometry where both Bi_2O_3 diffusivity into the substrate and evaporation can occur during the thermal treatment in a gas flow [11]. We believe once the decomposition of BFO films is triggered within the temperature instability range of the $BiFeO_3$ phase, it becomes further enhanced by diffusion of Bi^{3+} ions toward the substrate. Since higher diffusion rates of bismuth at elevated temperatures or prolonged annealing time increase Bi deficiency in the film, large amounts of secondary phases form whereby Bi-rich phase segregates inside the substrate and Fe-rich phase remains in the films. Therefore, incorporation of Bi excess up to 30 % in the precursor solution to compensate for the Bi_2O_3 loss resulted in a significantly lower amount of secondary phases and improved BFO stability which is in accordance with previous studies on Bi excess in chemical solution-deposited BFO films [27, 28]. Finally, our results suggest that substitution of Fe by aliovalent Ti can be another approach for stabilizing the BFO phase. Bernardo et al. reported on similar effect when Ti^{4+} is added into BFO ceramic [60, 61], although in studies of Valant et al. the Ti^{4+} ion is considered as an impurity leading to the appearance of a larger fraction of the iron-rich $Bi_2Fe_4O_9$ phase [7]. The plausible explanation for the improved phase stability of Ti-substituted films could be related to the limitation of bismuth diffusion due to reported segregation of titanium at the grain boundaries [61].

Magnetic properties

In order to study the influence of secondary phases and substitution of Fe by aliovalent Ti on the magnetic properties, three-layered BFO films annealed at 600 °C/1 h and 700 °C/1 h as well as $BiFe_{1-x}Ti_xO_3$ (where $x = 0.05$; 0.20) films were subjected to SQUID measurements at 300 K with the magnetic field parallel to the film surface. The obtained magnetic hysteresis loops are presented in Fig. 13. Both BFO films annealed at 600 and 700 °C show a weak ferromagnetic response. Bulk $BiFeO_3$ is an antiferromagnetic material with G-type magnetization and Néel temperature of 370 °C [3, 4, 17]. However, in thin films, a weak ferromagnetic response is often reported in $BiFeO_3$ and is associated with canting of Fe atoms in the antiferromagnetic lattice [67, 68]. In comparison with the film treated at 600 °C, the hysteresis loop of the BFO film annealed at 700 °C exhibits lower magnetization values. The observed behavior could be explained by the combination of two effects: a lower amount of $BiFeO_3$ phase due to decomposition at 700 °C as well as the presence of $Bi_2Fe_4O_9$ phase in the form of large grains (as evidenced by XRD and SEM) which exhibits paramagnetic behavior [69]. In the case of $BiFe_{1-x}Ti_xO_3$ films (where $x = 0.05$; 0.20), the saturation magnetization decreases further in comparison to BFO films annealed at 700 °C. Wang et al.

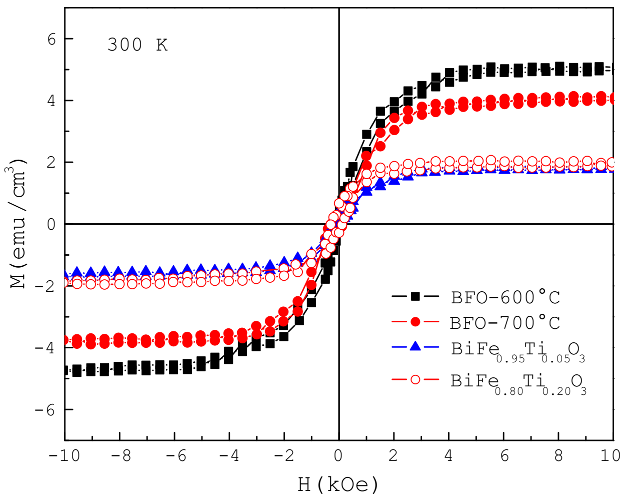

Fig. 13 Magnetic hysteresis loops of $BiFeO_3$ films annealed at 600 °C/700 °C and $BiFe_{1-x}Ti_xO_3$ ($x \leq 0.2$) films annealed at 700 °C measured at 300 K

[62] also observed weakened ferromagnetism in Ti-substituted films while Murari et al. [70] reported on paramagnetic behavior in BFO films substituted with 5 % Ti, relating these results to the non-magnetic nature of Ti^{4+} ions. In contrast with their films, the $BiFe_{0.95}Ti_{0.05}O_3$ films in the study presented here comprise $Bi_2Fe_4O_9$ as secondary phase which should also be taken into account when comparing the magnetic behavior. Also, the amount of this secondary phase in the $BiFe_{0.80}Ti_{0.20}O_3$ films, according to XRD results, is almost negligible. As it is seen in Fig. 13, compared with the BFO films annealed at 700 °C, the saturation magnetization of the Ti-substituted films appears at lower fields which can be an evidence of altering magnetic properties by substitution of Fe with aliovalent Ti.

Conclusions

Our study on the thermal stability of $BiFeO_3$ films obtained by CSD showed that a significant amount of the iron-rich $Bi_2Fe_4O_9$ phase formed at 700 °C as a result of $BiFeO_3$ film decomposition. The obtained results suggest a loss of Bi from films at higher temperatures, possibly not only due to volatilization but also due to high diffusion toward the substrate and possible interaction with the Pt electrode. In order to suppress the decomposition of $BiFeO_3$ and the formation of iron-rich phase, a shorter annealing time or the addition of Bi up to 30 mol% should be taken into account. Another approach for improving the stability of the BFO phase is substitution of Fe by aliovalent Ti where limitation of Bi diffusion probably occurs due to the inhibition of oxygen vacancy formation. These findings could be applicable not only to the other thin films with Bi-based compounds but also to films that contain other highly diffusible compounds when control over phase formation is crucial. Magnetic measurements revealed that presence of the $Bi_2Fe_4O_9$ secondary phase as well as substitution of Fe with Ti in BFO films leads to a decrease in saturation magnetization.

Acknowledgements The authors gratefully thank the support from Research Foundation Flanders (FWO Vlaanderen—research project G 0394.14 N.) and KU Leuven Concerted Research Action (GOA 14/007). C. De Dobbelaere is a postdoctoral research fellow of the Research Foundation Flanders. We also acknowledge Bart Ruttens (Institute for Materials Research, UHasselt) for his help with XRD and SEM measurements.

References

1. Catalan G, Scott JF (2009) Physics and applications of bismuth ferrite. Adv Mater 21(24):2463–2485. doi:10.1002/adma.200802849
2. Arnold DC, Knight KS, Morrison FD, Lightfoot P (2009) Ferroelectric-paraelectric transition in $BiFeO_3$: crystal structure of the orthorhombic beta phase. Phys Rev Lett 102(2):027602. doi:10.1103/PhysRevLett.102.027602
3. Selbach SM, Tybell T, Einarsrud MA, Grande T (2008) The ferroic phase transitions of $BiFeO_3$. Adv Mater 20(19): 3692–3696. doi:10.1002/adma.200800218
4. Palewicz A, Przenioslo R, Sosnowska I, Hewat AW (2007) Atomic displacements in $BiFeO_3$ as a function of temperature: neutron diffraction study. Acta Crystallogr Sect B-Struct Sci 63:537–544. doi:10.1107/s0108768107023956
5. Achenbac GD, James WJ, Gerson R (1967) Preparation of single-phase polycrystalline $BiFeO_3$. J Am Ceram Soc 50(8):437. doi:10.1111/j.1151-2916.1967.tb15153.x
6. Selbach SM, Einarsrud MA, Grande T (2009) On the thermodynamic stability of $BiFeO_3$. Chem Mater 21(1):169–173. doi:10.1021/cm802607p
7. Valant M, Axelsson AK, Alford N (2007) Peculiarities of a solid-state synthesis of multiferroic polycrystalline $BiFeO_3$. Chem Mater 19(22):5431–5436. doi:10.1021/cm071730+
8. Morozov MI, Lomanova NA, Gusarov VV (2003) Specific features of $BiFeO_3$ formation in a mixture of bismuth(III) and iron(III) oxides. Russ J Gen Chem 73(11):1676–1680. doi:10.1023/b:rugc.0000018640.30953.70
9. Bea H, Bibes M, Fusil S, Bouzehouane K, Jacquet E, Rode K, Bencok P, Barthelemy A (2006) Investigation on the origin of the magnetic moment of $BiFeO_3$ thin films by advanced X-ray characterizations. Phys Rev B 74(2):020101–020104. doi:10.1103/PhysRevB.74.020101
10. Filip'ev VS, Smolyaninov NP, Fesenko EG, Belyaev IN (1960) Synthesis of $BiFeO_3$ and determination of the unit cell. Kristallografiya 5(6):958
11. Selbach SM, Tybell T, Einarsrud MA, Grande T (2010) Phase transitions, electrical conductivity and chemical stability of $BiFeO_3$ at high temperatures. J Solid State Chem 183(5): 1205–1208. doi:10.1016/j.jssc.2010.03.014
12. Palai R, Katiyar RS, Schmid H, Tissot P, Clark SJ, Robertson J, Redfern SAT, Catalan G, Scott JF (2008) Beta phase and gamma-beta metal-insulator transition in multiferroic $BiFeO_3$. Phys Rev B 77(1):014110–014120. doi:10.1103/PhysRevB.77.014110

13. Maitre A, Francois M, Gachon JC (2004) Experimental study of the Bi_2O_3-Fe_2O_3 pseudo-binary system. J Phase Equilib Diffus 25(1):59–67. doi:10.1361/10549710417687
14. Rojac T, Bencan A, Malic B, Tutuncu G, Jones JL, Daniels JE, Damjanovic D (2014) $BiFeO_3$ ceramics: processing, electrical, and electromechanical properties. J Am Ceram Soc 97(7): 1993–2011. doi:10.1111/jace.12982
15. Bucci JD, Robertso BK, James WJ (1972) Precision determination of lattice parameters and coefficients of thermal expansion of $BiFeO_3$. J Appl Crystallogr 5(JUN1):187–191. doi:10.1107/s0021889872009173
16. Rojac T, Kosec M, Budic B, Setter N, Damjanovic D (2010) Strong ferroelectric domain-wall pinning in $BiFeO_3$ ceramics. J Appl Phys 108(7):174107–174114. doi:10.1063/1.3490249
17. Wang J, Neaton JB, Zheng H, Nagarajan V, Ogale SB, Liu B, Viehland D, Vaithyanathan V, Schlom DG, Waghmare UV, Spaldin NA, Rabe KM, Wuttig M, Ramesh R (2003) Epitaxial $BiFeO_3$ multiferroic thin film heterostructures. Science 299(5613):1719–1722. doi:10.1126/science.1080615
18. Bea H, Bibes M, Barthelemy A, Bouzehouane K, Jacquet E, Khodan A, Contour JP, Fusil S, Wyczisk F, Forget A, Lebeugle D, Colson D, Viret M (2005) Influence of parasitic phases on the properties of $BiFeO_3$ epitaxial thin films. Appl Phys Lett 87(7):072508–072510. doi:10.1063/1.2009808
19. Ihlefeld JF, Kumar A, Gopalan V, Schlom DG, Chen YB, Pan XQ, Heeg T, Schubert J, Ke X, Schiffer P, Orenstein J, Martin LW, Chu YH, Ramesh R (2007) Adsorption-controlled molecular-beam epitaxial growth of $BiFeO_3$. Appl Phys Lett 91(7):071922–071924. doi:10.1063/1.2767771
20. Das RR, Kim DM, Baek SH, Eom CB, Zavaliche F, Yang SY, Ramesh R, Chen YB, Pan XQ, Ke X, Rzchowski MS, Streiffer SK (2006) Synthesis and ferroelectric properties of epitaxial $BiFeO_3$ thin films grown by sputtering. Appl Phys Lett 88(24):242904–242906. doi:10.1063/1.2213347
21. Zheng R, Gao X, Wang J, Ramakrishna S (2008) Multiferroic $BiFeO_3$ thin films buffered by a $SrRuO_3$ layer. J Am Ceram Soc 91(2):463–466. doi:10.1111/j.1551-2916.2007.02128.x
22. Lee CC, Wu LJ, Wu JM (2007) Studies on forming gas annealing treated $BiFeO_3$ thin films and capacitors. Appl Phys Lett 91(20):202902–202904. doi:10.1063/1.2806191
23. Yang SY, Zavaliche F, Mohaddes-Ardabili L, Vaithyanathan V, Schlom DG, Lee YJ, Chu YH, Cruz MP, Zhan Q, Zhao T, Ramesh R (2005) Metalorganic chemical vapor deposition of lead-free ferroelectric $BiFeO_3$ films for memory applications. Appl Phys Lett 87(10):102903–102905. doi:10.1063/1.2041830
24. Wang Y, Jiang QH, He HC, Nan CW (2006) Multiferroic $BiFeO_3$ thin films prepared via a simple sol-gel method. Appl Phys Lett 88(14):142503–142505. doi:10.1063/1.2191947
25. Qi XD, Dho JH, Blamire M, Jia QX, Lee JS, Foltyn S, MacManus-Driscoll JL (2004) Epitaxial growth of $BiFeO_3$ thin films by LPE and sol-gel methods. J Magn Magn Mater 283(2–3):415–421. doi:10.1016/j.jmmm.2004.06.014
26. Singh SK, Kim YK, Funakubo H, Ishiwara H (2006) Epitaxial $BiFeO_3$ thin films fabricated by chemical solution deposition. Appl Phys Lett 88(16):162904–162906. doi:10.1063/1.2196477
27. Casper MD, Losego MD, Maria JP (2013) Optimizing phase and microstructure of chemical solution-deposited bismuth ferrite ($BiFeO_3$) thin films to reduce DC leakage. J Mater Sci 48(4):1578–1584. doi:10.1007/s10853-012-6914-0
28. Tyholdt F, Jorgensen S, Fjellvag H, Gunnaes AE (2005) Synthesis of oriented $BiFeO_3$ thin films by chemical solution deposition: phase, texture, and microstructural development. J Mater Res 20(8):2127–2139. doi:10.1577/jmr.2005.0263
29. Yakovlev S, Zekonyte J, Solterbeck CH, Es-Souni M (2005) Interfacial effects on the electrical properties of multiferroic $BiFeO_3$/Pt/Si thin film heterostructures. Thin Solid Films 493(1–2):24–29. doi:10.1016/j.tsf.2005.06.020
30. Liu KH, Cai W, Fu CL, Lei K, Xiang L, Gong XB (2014) Preparation and electric properties of $BiFeO_3$ film by electrophoretic deposition. J Alloys Compd 605:21–28. doi:10.1016/j.jallcom.2014.03.161
31. Toupet H, Le Marrec F, Holc J, Kosec M, Vilarhino P, Karkut MG (2009) Growth and thermal stability of epitaxial $BiFeO_3$ thin films. J Magn Magn Mater 321(11):1702–1705. doi:10.1016/j.jmmm.2009.02.024
32. Fujino S, Murakami M, Lim SH, Wuttig M, Salamanca-Riba LG, Takeuchi I (2007) Ferroelectric properties of multiphase Bi-Fe-O thin films. Solid State Ion 178(21–22):1257–1261. doi:10.1016/j.ssi.2007.07.004
33. Calzada ML, Gonzalez A, Garcia-Lopez J, Jimenez R (2003) Crystallization, heterostructure, microstructure, and properties of ferroelectric strontium bismuth tantalate films derived from tantalum glycolate solutions. Chem Mater 15(25):4775–4783. doi:10.1021/cm031065e
34. Schwartz RW (1997) Chemical solution deposition of perovskite thin films. Chem Mater 9(11):2325–2340. doi:10.1021/cm970286f
35. Hardy A, Gielis S, Van den Rul H, D'Haen J, Van Bael MK, Mullens J (2009) Effects of precursor chemistry and thermal treatment conditions on obtaining phase pure bismuth ferrite from aqueous gel precursors. J Eur Ceram Soc 29(14):3007–3013. doi:10.1016/j.jeurceramsoc.2009.05.018
36. Hardy A, D'Haen J, Van Bael MK, Mullens J (2007) An aqueous solution-gel citratoperoxo-Ti(IV) precursor: synthesis, gelation, thermo-oxidative decomposition and oxide crystallization. J Sol-Gel Sci Technol 44(1):65–74. doi:10.1007/s10971-007-1601-3
37. Van Bael MK, Nelis D, Hardy A, Mondelaers D, Van Werde K, D'Haen J, Vanhoyland G, Van den Rul H, Mullens J, Van Poucke LC, Frederix F, Wouters DJ (2002) Aqueous chemical solution deposition of ferroelectric thin films. Integr Ferroelectr 45:113–122. doi:10.1080/10584580190044010
38. Schwartz RW, Schneller T, Waser R (2004) Chemical solution deposition of electronic oxide films. CR Chim 7(5):433–461. doi:10.1016/j.crci.2004.01.007
39. Calzada ML, Jimenez R, Gonzalez A, Garcia-Lopez J, Leinen D, Rodriguez-Castellon E (2005) Interfacial phases and electrical characteristics of ferroelectric strontium bismuth tantalate films on Pt/TiO_2 and Ti/Pt/Ti heterostructure electrodes. Chem Mater 17(6):1441–1449. doi:10.1021/cm048996q
40. Stojakovic D (2012) Electron backscatter diffraction in materials characterization. Process Appl Ceram 6(1):1–13
41. Tyholdt F, Fjellvag H, Gunnaes AE, Olsen A (2007) Synthesis of epitaxial $BiFeO_3$ films by chemical solution deposition on Pt(100). J Appl Phys 102(7):074108–074114. doi:10.1063/1.2784999
42. Okamoto H (1991) The Bi-Pt (Bismuth-Platinum) system. J Phase Equilib 12(2):207–210. doi:10.1007/BF02645718
43. Bretos I, Jimenez R, Rodriguez-Castellon E, Garcia-Lopez J, Calzada ML (2008) Heterostructure and compositional depth profile of low-temperature processed lead titanate-based ferroelectric thin films prepared by photochemical solution deposition. Chem Mater 20(4):1443–1450. doi:10.1021/cm7025812
44. Dippel AC, Schneller T, Waser R, Park D, Mayer J (2010) Formation sequence of lead platinum interfacial phases in chemical solution deposition derived $Pb(Zr_{1-x}Ti_x)O_3$ thin films. Chem Mater 22(23):6209–6211. doi:10.1021/cm101195t
45. Zhang X, Bourgeois L, Yao J, Wang H, Webley PA (2007) Tuning the morphology of bismuth ferrite nano- and microcrystals: from sheets to fibers. Small 3(9):1523–1528. doi:10.1002/smll.200700182

46. Han JT, Huang YH, Wu XJ, Wu CL, Wei W, Peng B, Huang W, Goodenough JB (2006) Tunable synthesis of bismuth ferrites with various morphologies. Adv Mater 18(16):2145–2148. doi:10.1002/adma.200600072
47. Ruan QJ, Zhang WD (2009) Tunable morphology of $Bi_2Fe_4O_9$ crystals for photocatalytic oxidation. J Phys Chem C 113(10): 4168–4173. doi:10.1021/jp810098f
48. Tsai CJ, Yang CY, Liao YC, Chueh YL (2012) Hydrothermally grown bismuth ferrites: controllable phases and morphologies in a mixed KOH/NaOH mineralizer. J Mater Chem 22(34): 17432–17436. doi:10.1039/c2jm33859a
49. Hu ZT, Chen B, Lim TT (2014) Single-crystalline $Bi_2Fe_4O_9$ synthesized by low-temperature co-precipitation: performance as photo- and Fenton catalysts. RSC Adv 4(53):27820–27829. doi:10.1039/c4ra02555e
50. Zhang XY, Lv J, Bourgeois L, Cui JW, Wu YC, Wang HT, Webley PA (2011) Formation and photocatalytic properties of bismuth ferrite submicrocrystals with tunable morphologies. New J Chem 35(4):937–941. doi:10.1039/c1nj00008j
51. Lahmar A, Zhao K, Habouti S, Dietze M, Solterbeck CH, Es-Souni M (2011) Off-stoichiometry effects on $BiFeO_3$ thin films. Solid State Ion 202(1):1–5. doi:10.1016/j.ssi.2011.03.017
52. Singh SK, Funakuba H, Uchida H, Ishiwara H (2005) Structural and electrical properties of $BiFeO_3$ thin films. Integr Ferroelectr 76:139–146. doi:10.1080/10584580500413855
53. Kalantari K, Sterianou I, Karimi S, Ferrarelli MC, Miao S, Sinclair DC, Reaney IM (2011) Ti-doping to reduce conductivity in $Bi_{0.85}Nd_{0.15}FeO_3$ ceramics. Adv Funct Mater 21(19):3737–3743. doi:10.1002/adfm.201100191
54. Yasui S, Uchida H, Nakaki H, Nishida K, Funakubo H, Koda S (2007) Analysis for crystal structure of Bi(Fe, Sc)O3 thin films and their electrical properties. Appl Phys Lett 91(2):022906–022908. doi:10.1063/1.2756356
55. Chung CF, Lin JP, Wu JM (2006) Influence of Mn and Nb dopants on electric properties of chemical-solution-deposited $BiFeO_3$ films. Appl Phys Lett 88(24):242909–242911. doi:10.1063/1.2214138
56. Do D, Kim JW, Kim SS (2011) Effects of Dy and Mn codoping on ferroelectric properties of $BiFeO_3$ thin films. J Am Ceram Soc 94(9):2792–2795. doi:10.1111/j.1551-2916.2011.04720.x
57. Yan F, Lai MO, Lu L, Zhu TJ (2010) Enhanced multiferroic properties and valence effect of Ru-doped $BiFeO_3$ thin films. J Phys Chem C 114(15):6994–6998. doi:10.1021/jp1009127
58. Khomchenko VA, Kiselev DA, Kopcewicz M, Maglione M, Shvartsman VV, Borisov P, Kleemann W, Lopes AML, Pogorelov YG, Araujo JP, Rubinger RM, Sobolev NA, Vieira JM, Kholkin AL (2009) Doping strategies for increased performance in $BiFeO_3$. J Magn Magn Mater 321(11):1692–1698. doi:10.1016/j.jmmm.2009.02.008
59. Wu JG, Wang J (2010) Ferroelectric and impedance behavior of La- and Ti-codoped $BiFeO_3$ thin films. J Am Ceram Soc 93(9):2795–2803. doi:10.1111/j.1551-2916.2010.03816.x
60. Bernardo MS, Jardiel T, Peiteado M, Caballero AC, Villegas M (2011) Sintering and microstructural characterization of W^{6+}, Nb^{5+} and Ti^{4+} iron-substituted $BiFeO_3$. J Alloys Compd 509(26):7290–7296. doi:10.1016/j.jallcom.2011.04.087
61. Bernardo MS, Jardiel T, Peiteado M, Mompean FJ, Garcia-Hernandez M, Garcia MA, Villegas M, Caballero AC (2013) Intrinsic compositional inhomogeneities in bulk Ti-doped $BiFeO_3$: microstructure development and multiferroic properties. Chem Mater 25(9):1533–1541. doi:10.1021/cm303743h
62. Wang Y, Nan CW (2006) Enhanced ferroelectricity in Ti-doped multiferroic $BiFeO_3$ thin films. Appl Phys Lett 89(5): 052903–052905. doi:10.1063/1.2222242
63. Zheng CD, Yu J, Zhang DM, Yang B, Wu YY, Wang LH, Wang YB, Zhou WL (2007) Processing and ferroelectric properties of Ti-doped $BiFeO_3$ ceramics. Integr Ferroelectr 94:31–36. doi:10.1080/10584580701755872
64. Hu GD, Fan SH, Yang CH, Wu WB (2008) Low leakage current and enhanced ferroelectric properties of Ti and Zn codoped $BiFeO_3$ thin film. Appl Phys Lett 92(19):192905–192907. doi:10.1063/1.2918130
65. Chan HM, Harmer MP, Smyth DM (1986) Compensating defects in highly donor-doped $BaTiO_3$. J Am Ceram Soc 69(6):507–510. doi:10.1111/j.1151-2916.1986.tb07453.x
66. Bernardo MS, Jardiel T, Peiteado M, Caballero AC, Villegas M (2011) Reaction pathways in the solid state synthesis of multiferroic $BiFeO_3$. J Eur Ceram Soc 31(16):3047–3053. doi:10.1016/j.jeurceramsoc.2011.03.018
67. Bea H, Bibes M, Petit S, Kreisel J, Barthelemy A (2007) Structural distortion and magnetism of $BiFeO_3$ epitaxial thin films: a Raman spectroscopy and neutron diffraction study. Philos Mag Lett 87(3–4):165–174. doi:10.1080/09500830701235802
68. Ederer C, Spaldin NA (2005) Weak ferromagnetism and magnetoelectric coupling in bismuth ferrite. Phys Rev B 71(6):060401–060404. doi:10.1103/PhysRevB.71.060401
69. Tian ZM, Yuan SL, Wang XL, Zheng XF, Yin SY, Wang CH, Liu L (2009) Size effect on magnetic and ferroelectric properties in $Bi_2Fe_4O_9$ multiferroic ceramics. J Appl Phys 106(10): 103912–103915. doi:10.1063/1.3259392
70. Murari NM, Thomas R, Melgarejo RE, Pavunny SP, Katiyar RS (2009) Structural, electrical, and magnetic properties of chemical solution deposited $BiFe_{1-x}Ti_xO_3$ and $BiFe_{0.9}Ti_{0.05}Co_{0.05}O_3$ thin films. J Appl Phys 106(1):014103–014107. doi:10.1063/1.3158556